

Millimeter-Wave Integrated-Horn Antennas: Part I—Theory

George V. Eleftheriades, *Student Member, IEEE*, Walid Y. Ali-Ahmad, *Student Member, IEEE*,
Linda P. B. Katehi, *Senior Member, IEEE*, and Gabriel M. Rebeiz, *Member, IEEE*

Abstract—Dipole excited integrated horn antennas etched in Si/GaAs are a very promising class of antennas for millimeter and submillimeter applications. Areas of application include imaging and tracking through rain and fog, remote sensing, radio astronomy, and plasma diagnostics. In this paper (Part I), the far-field pattern and input impedance of a dipole-fed horn antenna in a ground plane are calculated using full-wave analysis. The solution is based on the numerical evaluation of the pertinent Green's function for the horn structure and the application of the method of moments. The convergence characteristics of the full-wave analysis method are investigated, along with the resonant properties of the strip-dipole and the corresponding behavior of the far-field patterns. The theoretical results are compared in Part II with microwave and millimeter-wave measurements.

I. INTRODUCTION

INTEGRATED horn antennas consist of a dipole-antenna suspended on a $1 \mu\text{m}$ dielectric membrane inside a pyramidal cavity etched in silicon. The antennas are fully integrated, free of dielectric and surface-wave losses, and easily reproducible for array applications. Single and dual-polarized two-dimensional arrays of integrated horn antennas have been extensively investigated at 94 GHz [1]–[3]. These arrays are used for millimeter-wave imaging and multibeam communication applications. The horn antennas are typically between 1λ -square and 1.5λ -square, and show excellent patterns with a directivity around 10–12 dB. Integrated-horn antennas are very efficient, with a measured aperture efficiency of 72% for a 1λ -square horn in a two-dimensional array [4].

The analysis done so far on integrated horn antennas concentrated on calculating the far-field radiation pattern of a horn antenna in a two-dimensional infinite array. The patterns were calculated by employing reciprocity and Floquet-mode representation of the free-space field [1]. However, since the analysis was performed in the receiving mode, this method could not be applied to the calculation of the input impedance and resonant length of the dipole antenna inside the cavity. Also, there is considerable interest in single-channel receivers employing a single integrated-horn antenna. Again, the analysis method described above cannot be used since the free-space field is not represented anymore by

Manuscript received November 26, 1990; revised July 12, 1991. This work was supported by NASA/Center for Space Terahertz Technology at the University of Michigan.

The authors are with the NASA/Center for Space Terahertz Technology and the Department of Electrical Engineering and Computer Science, The University of Michigan, Ann Arbor, MI 48109.

IEEE Log Number 9103275.

Floquet-modes. In this paper, a full-wave analysis of a dipole-fed horn antenna in a ground plane is presented. The pertinent Green's function is obtained by treating the horn as a multisteped waveguide discontinuity. The transition to free-space is rigorously modeled by matching to the Fourier plane wave representation of the free-space field. The calculated Green's function is used to set an integral equation for the strip-dipole current enabling the evaluation of the input impedance and the resonant properties of the feeding strip. The aperture field is also found, and the far-field patterns are calculated from its Fourier transform. The convergence characteristics of the method along with certain properties pertinent only to dipole-fed horn antennas are discussed.

II. THEORETICAL FORMULATION

The theoretical study of the integrated horn antenna is based on a space-domain integral equation approach. This approach has been previously applied to several planar structures [5]–[7] and has shown good accuracy and satisfactory computational efficiency.

A. Integral Equation

Consider the horn shown in Fig. 1. The excitation is provided through a center-fed strip dipole oriented along the \hat{y} -direction. The walls of the pyramidal silicon horn structure are covered with evaporated gold, and considered perfectly conducting. The feeding dipole is modeled by an infinitesimally thin and perfectly conducting strip of width w .

The electric field inside the horn may be written in terms of the electric current on the strip dipole as shown below:

$$\bar{E} = \int_{S_d} \bar{G} \cdot \bar{J} dx' dy' \quad (1)$$

where \bar{G} is the modified dyadic Green's function for the structure and S_d is the surface of the strip dipole. Since the only unknown in (1) is the current in the strip conductor, the Green's function has to satisfy all the boundary conditions except the ones that apply on the dipole surface. Due to the complicated geometry of the horn, the Green's function cannot be expressed in a closed form as is the case with all previously solved planar structures [5]–[8]. The Green's function can only be evaluated numerically and details of its derivation are presented below.

B. Derivation of the Green's Function

In order to evaluate the Green's function, the horn is approximated by a multisteped discontinuity of waveguide

Indexes 0, I, II, N in (5) denote the apex, source (left), source (right), and aperture waveguide section, respectively. It is assumed that there are no reflections from the apex section since the fields in this section are strongly evanescent. An additional relation between the waves a^N, b^N of the aperture section is obtained by matching the field on the aperture waveguide section to free space. The free-space field is represented by a plane wave Fourier expansion. From the continuity of the electric and magnetic fields over the aperture of the horn we obtain (6) and (7), respectively:

$$\begin{aligned} & \sum_{ij} \frac{\bar{e}_{ij}^{N,TE}(x,y)}{\sqrt{Y_{ij}^{N,TE}}} (a_{ij}^{N,TE} + b_{ij}^{N,TE}) \\ & + \sum_{ij} \frac{\bar{e}_{ij}^{N,TM}(x,y)}{\sqrt{Y_{ij}^{N,TM}}} (a_{ij}^{N,TM} + b_{ij}^{N,TM}) \\ & = \frac{1}{2\pi} \int_{-\infty}^{\infty} \int_{-\infty}^{\infty} \bar{g}_t(k_x, k_y) e^{-jk_x x} e^{-ik_y y} dk_x dk_y \quad (6) \\ & \sum_{ij} \bar{e}_{ij}^{N,TE}(x,y) \sqrt{Y_{ij}^{N,TE}} (b_{ij}^{N,TE} - a_{ij}^{N,TE}) \\ & + \sum_{ij} \bar{e}_{ij}^{N,TM}(x,y) \sqrt{Y_{ij}^{N,TM}} (b_{ij}^{N,TM} - a_{ij}^{N,TM}) \\ & = -\frac{1}{2\pi\omega\mu_0} \int_{-\infty}^{\infty} \int_{-\infty}^{\infty} \hat{z} \\ & \quad \times (\bar{k} \times \bar{g}) e^{-ik_x x} e^{-ik_y y} dk_x dk_y. \quad (7) \end{aligned}$$

The plane wave spectrum of the free-space field $\bar{g}(k_x, k_y)$ is eliminated between the two equations by Fourier transforming the first equation and substituting in the second equation. This provides the required relation among the coefficients of the aperture section:

$$[F_{11} \quad F_{22}] \begin{bmatrix} a_N \\ b_N \end{bmatrix} = \begin{bmatrix} 0 \\ 0 \end{bmatrix}. \quad (8)$$

The block matrices F_{11} and F_{22} contain spectral integrals between the modes of the aperture section. To avoid numerical integrations having infinite limits, the integrals were transformed into the space-domain using Parseval's theorem (see Appendix). The aperture and apex fields are transferred to the source section using (5) and (8). This reduces the problem to finding the fields in a waveguide section which is excited by a Hertzian dipole and terminated by two multimode loads (see Fig. 3):

$$\text{scattering matrix of load } Z_{L1}: b^I = S_{22}^B a^I \quad (9)$$

$$\text{scattering matrix of load } Z_{L2}: b^{II} = Q a^{II} \quad (10)$$

where

$$Q = S_{11}^A - S_{12}^A (F_{11} + F_{22} S_{22}^A)^{-1} F_{22} S_{21}^A. \quad (11)$$

The multimode loads Z_{L1}, Z_{L2} are explicitly known, and the fields in the source waveguide section can be completely determined by matching over the source interface. The matching procedure yields

$$a^I = b^{II} - \hat{e}(x', y') \quad (12)$$

$$b^I = a^{II} + \hat{e}(x', y') \quad (13)$$

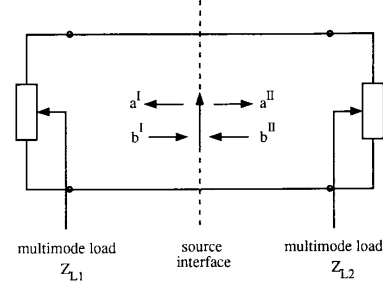


Fig. 3. The reduced problem in which a Hertzian dipole excites the source waveguide section which is terminated by two multimode loads.

where

$$\hat{e}(x', y') = \begin{bmatrix} \frac{e^{II,TE}(x', y')}{2\sqrt{Y_{mn}^{II,TE}}} \\ \frac{e^{II,TM}(x', y')}{2\sqrt{Y_{mn}^{II,TM}}} \end{bmatrix} \quad (14)$$

and (x', y') is the location of the Hertzian dipole on the source plane. Using (12) and (13) along with the scattering matrices of loads Z_{L1} and Z_{L2} defined in (9) and (10), the wave amplitudes a^{II} and b^{II} are evaluated by

$$a^{II} = P \hat{e}(x', y') \quad (15)$$

$$b^{II} = Q P \hat{e}(x', y') \quad (16)$$

where

$$P = (S_{22}^B Q - I)^{-1} (S_{22}^B + I). \quad (17)$$

The transverse electric field on the source interface is transformed from its summation form of (2) into the matrix form:

$$\bar{E}_t = \begin{bmatrix} \frac{\bar{e}_{mn}^{II,TE}(x,y)}{\sqrt{Y_{mn}^{II,TE}}} & \frac{\bar{e}_{mn}^{II,TM}(x,y)}{\sqrt{Y_{mn}^{II,TM}}} \end{bmatrix} \cdot \begin{bmatrix} a_{mn}^{II,TE} + b_{mn}^{II,TE} \\ a_{mn}^{II,TM} + b_{mn}^{II,TM} \end{bmatrix}. \quad (18)$$

In (18) the dependence of the field on the Hertzian dipole source is implicitly included in the wave coefficients a_{mn}^{II} and b_{mn}^{II} . Therefore, the transverse component of the Green's function inside the source waveguide section is obtained by substituting (15)–(17) into (18):

$$G_{yy}(x, y, x', y') = \begin{bmatrix} \frac{\bar{e}_{ymn}^{II,TE}(x,y)}{\sqrt{Y_{mn}^{II,TE}}} & \frac{\bar{e}_{ymn}^{II,TM}(x,y)}{\sqrt{Y_{mn}^{II,ME}}} \end{bmatrix} \cdot \left[\frac{(Q + I)P}{2} \right] \begin{bmatrix} \frac{\bar{e}_{ymn}^{II,TE}(x', y')}{\sqrt{Y_{mn}^{II,TE}}} \\ \frac{\bar{e}_{ymn}^{II,TM}(x', y')}{\sqrt{Y_{mn}^{II,ME}}} \end{bmatrix}. \quad (19)$$

The required Green's function is in a quadratic form which is also symmetric (complying with reciprocity requirements). The kernel of the quadratic form is not given in a closed form, and can only be evaluated numerically using (11) and (17).

C. Evaluation of the Current Distribution

The electric field in the source waveguide section due to a narrow dipole strip is found by the superposition integral:

$$E_y(x, y) = \int_{Sd} \bar{G}_{yy}(x, y, x', y') W(x') J_y(y') dx' dy' \quad (20)$$

where Sd is the strip-dipole surface. The transverse current distribution is chosen to satisfy the edge condition [7], [14]:

$$W(x) = \frac{\frac{2}{\pi w}}{\sqrt{1 - \left[\frac{2(x - x_0)}{w} \right]^2}} \quad \text{on the strip surface} \quad (21)$$

where (x_0, y_0) are the coordinates of the center of the strip and w is its width. The longitudinal current distribution is expanded into a series of subsectional sinusoidal pulses:

$$J_y(y) = \sum_{k=1}^{N_b} I_k f_k(y) \quad (22)$$

where $f_k(y)$

$$= \begin{cases} \frac{\sin [2\pi(\Delta y - |y - y_k|)]}{\sin(2\pi\Delta y)} & \text{if } |y - y_k| \leq \Delta y \\ 0 & \text{otherwise.} \end{cases} \quad (23)$$

y_k is the coordinate of the center of the k th subsection, Δy is the subsectional length ($y_{k+1} - y_k$), and N_b is the number of pulses used. A delta gap generator of magnitude V_g is assumed to be applied at the center of the strip-dipole. The condition of zero electric field over the surface of the strip enables the formulation of an integral equation for the unknown current $J_y(y')$ which is solved by Galerkin's technique. The computed current distribution yields the input impedance and the resonance characteristics of the strip. The input impedance of the strip is found by

$$z_{in} = V_g / I(0) \quad (24)$$

where $I(0)$ is the computed value of the induced current at the center of the strip. The resonant length of the strip is defined as the length at which the input impedance has a vanishing reactive part.

The major difficulty in the above procedure is the numerical calculation of the Green's function. To obtain a computationally affordable scheme, the field in the source section is considered to be a superposition of a primary incident field due to the dipole source and a secondary field due to the reflections from the horn structure. Subsequently, the following simplifying assumption is made: it is assumed that higher order mode reflections from the horn structure on the source

plane (secondary field) are very small compared to the corresponding incident source field (primary field). Thus, in the calculation of the Green's function only a few secondary modes are retained whereas more primary modes are included. The pertinent primary field is the field of an infinitesimal dipole exciting an infinite waveguide:

$$G_{yy}^{\text{prim}}(x, y, x', y') = \begin{bmatrix} \frac{\bar{e}_{ymn}^{II, \text{TE}}(x, y)}{\sqrt{Y_{mn}^{II, \text{TE}}}} & \frac{\bar{e}_{ymn}^{II, \text{TM}}(x, y)}{\sqrt{Y_{mn}^{II, \text{ME}}}} \\ \frac{\bar{e}_{ymn}^{II, \text{TE}}(x', y')}{2\sqrt{Y_{mn}^{II, \text{TE}}}} & \frac{\bar{e}_{ymn}^{II, \text{TM}}(x', y')}{2\sqrt{Y_{mn}^{II, \text{ME}}}} \end{bmatrix} \cdot \begin{bmatrix} - \\ - \\ - \\ - \end{bmatrix} \quad (25)$$

In this way, the low-order part of the Green's function which contains both primary and secondary field is evaluated numerically using (19). For high-order modes, only the primary contribution to the Green's function is taken into consideration according to the closed form expression of (25).

D. Far-Field Patterns

The horn is excited by a center-fed dipole at resonance which was assumed to be equivalent to a Hertzian dipole located at the position of the center of the strip. The far-field patterns are subsequently evaluated from the asymptotic approximation of the plane-wave spectrum $\bar{g}(k_x, k_y)$ obtained from (6), [15].

III. CONVERGENCE CHARACTERISTICS

In this section the convergence characteristics of the strip-dipole resonant resistance and of the corresponding resonant length are examined. The validity of the approximations used in the theoretical model is tested and, at the same time, a feeling for the range of the various parameters involved in the analysis is acquired. In what follows, the horn under examination is assumed to be a typical integrated horn with a 70° flare angle, a square aperture of size 1.35 λ and excited by a strip dipole at a distance of 0.51 λ from the apex.

A. Convergence with Respect to the Number of Secondary Modes.

This type of convergence examines the validity of the assumption of small high-order reflections in the source section. The convergence diagram of the resonant length and resonant resistance as a function of the secondary modes retained is shown in Fig. 4. It is clear that at least 50 secondary modes are required in order to achieve results with acceptable accuracy. For different horn geometries the same procedure should be repeated in order to calculate the correct number of secondary modes required for convergence.

B. Convergence with Respect to the Number of Waveguide Sections

The convergence of the resonant length and the resonant resistance versus the number of waveguide sections is shown in Fig. 5. Since the horn under study has a large flare angle,

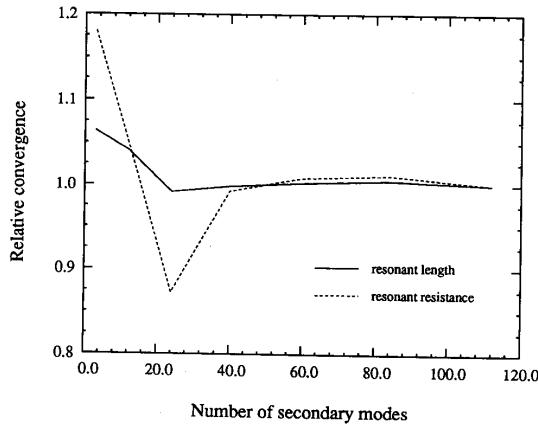


Fig. 4. Convergence with respect to the number of secondary modes retained in the numerical evaluation of the Green's function. (Up to the $TE_{55,55}$ and the $TM_{55,55}$ mode included in the primary field.)

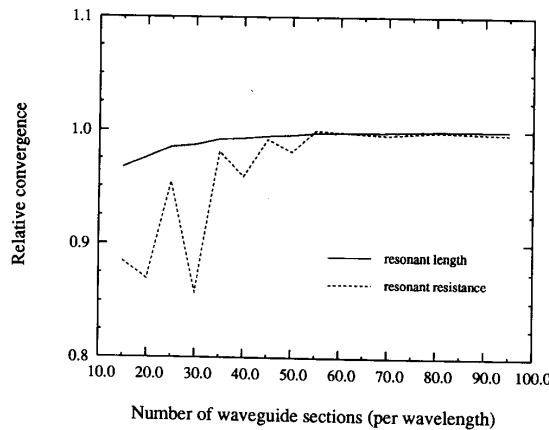


Fig. 5. Convergence with respect to the number of waveguide sections by which the horn is approximated.

the convergence diagram provides a safe universal estimation of the number of waveguide sections per wavelength required for convergence. It is evident that approximately 70 sections per wavelength are needed for reliable results.

IV. INTERESTING FEATURES OF DIPOLE-FED HORN ANTENNAS

A. Possibility of No Strip Resonances

The wedge termination of the horn at its apex sets up a cavity environment for the strip dipole, and the dominant mode generates a standing wave in the region enclosed between the dipole and the apex of the horn. Therefore, the strip-dipole encounters capacitive and inductive regions as it moves along the axis of the horn. The strip will not resonate if the limited strip length dictated by the geometry of the horn is not capable of providing adequate inductance in the capacitive regions. On the other hand, the strip will always resonate in the inductive regions because strips are very capacitive for short lengths. The above-mentioned behavior is characterized

both numerically and experimentally and the results can be found in the companion paper [3].

B. Real Input Impedance in the Cutoff Region

The cutoff region of the horn is defined as the region in the neighborhood of the apex where the cross section of the corresponding waveguide section is less than half a wavelength. Therefore, for a strip-dipole in the cutoff region all the waveguide modes around the strip are evanescent. Surprisingly enough, the numerically evaluated strip input impedance in this region has a small but nonzero real part. The same behavior is observed also experimentally, and the explanation lies in the fact that the linear combination of incident and reflected evanescent modes is capable of carrying real power. Indeed for the (m, n) mode, the real part of the Poynting vector is given by

$$\begin{aligned} & \frac{1}{2} \operatorname{Re} [E_{mn} \times H_{mn}^*] \\ &= \frac{1}{2} \operatorname{Re} \left[\frac{1}{\sqrt{Y_{mn}}} (a_{mn} e^{-\gamma_{mn} z} + b_{mn} e^{\gamma_{mn} z}) \right. \\ & \quad \left. \cdot \sqrt{Y_{mn}^*} (a_{mn}^* e^{-\gamma_{mn}^* z} - b_{mn}^* e^{\gamma_{mn}^* z}) \right] \\ &= \operatorname{Im} [a_{mn} b_{mn}^*]. \end{aligned} \quad (26)$$

If no reflections are present, then $b_{mn} = 0$ and then (m, n) mode does not carry any real power.

C. Effect of Dipole-Feed Position on the Far-Field Pattern

A centered vertical Hertzian dipole triggers the TE_{mn} ($m = 1, 3, 5, \dots, n = 0, 2, 4, \dots$) and the corresponding TM_{mn} ($m = 1, 3, 5, \dots, n = 2, 4, 6, \dots$) modes. This is exactly the same set of modes which is excited in a conventional waveguide-fed horn [9], [10]. For short distances of the feeding strip from the apex of the horn, the high-order modes are attenuated significantly before reaching the horn aperture and therefore the far-field patterns are similar to those of a corresponding TE_{10} waveguide-fed horn. However, as the dipole approaches the aperture of the horn, high-order modes can reach the aperture without significant attenuation, therefore distorting its field. The patterns for a typical 70° horn with an aperture of 1.35λ and dipole positions of 0.4λ and 0.8λ are shown in Fig. 6(a). The distribution of the aperture field for the 0.4λ position corresponds to the dominant TE_{10} mode [Fig. 6(b)]. For the 0.8λ position, higher order modes (mainly TE_{12}/TM_{12}) disturb significantly the dominant mode distribution [Fig. 6(c)]. This results in an increased phase error and a corresponding spreading of the E -plane pattern.

V. CONCLUSION

A full-wave analysis of a dipole-fed horn antenna using mode-matching and plane wave representation of the free-space field has been presented. Convergence studies on the full-wave analysis indicate that the horn should be modeled by approximately 70 sections per wavelength, and at least 50 secondary modes are needed for accurate results. The analysis indicates that the horn radiation pattern and the dipole

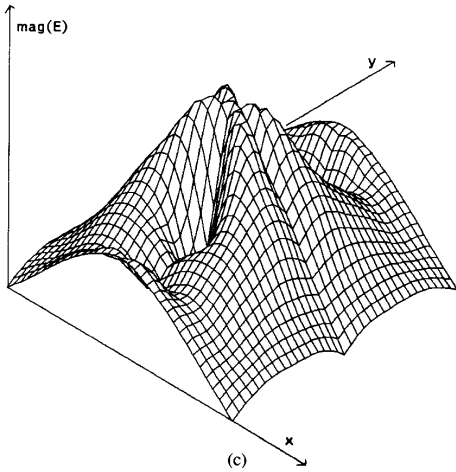
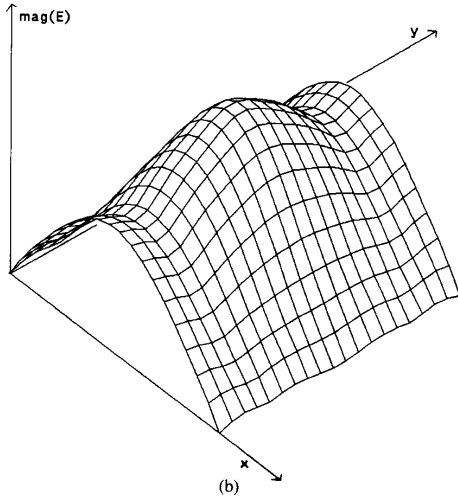
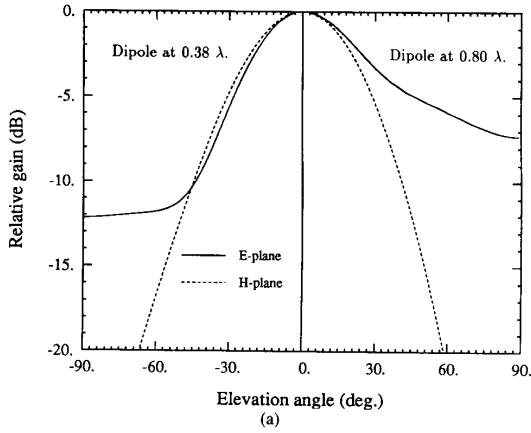


Fig. 6. (a) Far-field patterns for a 70° flare angle horn having a square aperture of 1.35λ and excited by a dipole at a distance 0.38λ away from the apex (left) and 0.80λ away from the apex (right). (b) Magnitude of the aperture E -field for the horn with the exciting dipole at 0.38λ away from its apex. (c) Same as (b) but with the exciting dipole at 0.80λ away from the apex.

input impedance are a strong function of the dipole position inside the cavity, and there is a possibility of no resonance for certain dipole positions. The experimental verification of the theory is presented in Part II [3].

VI. APPENDIX

A. Scattering Matrix of a Step Discontinuity

The scattering matrix for the waveguide discontinuity of Fig. 2 is being described in (4). The primitive matrix V appearing in (4) has the following form:

$$V = \begin{bmatrix} V^{EE} & V^{EM} \\ V^{ME} & V^{MM} \end{bmatrix} \quad (27)$$

where

$$V_{mnl}^{EE} = \sqrt{\frac{Y_{mn}^{i+1, TE}}{Y_{kl}^{i, TE}}} \int_{A^i} \bar{e}_{kl}^{i, TE} \cdot \bar{e}_{mn}^{i+1, TE} dA^i \quad (28)$$

$$V_{mnl}^{ME} = \sqrt{\frac{Y_{mn}^{i+1, TE}}{Y_{kl}^{i, TM}}} \int_{A^i} \bar{e}_{kl}^{i, TM} \cdot \bar{e}_{mn}^{i+1, TE} dA^i \quad (29)$$

$$V_{mnl}^{EM} = \sqrt{\frac{Y_{mn}^{i+1, TM}}{Y_{kl}^{i, TE}}} \int_{A^i} \bar{e}_{kl}^{i, TE} \cdot \bar{e}_{mn}^{i+1, TM} dA^i \quad (30)$$

$$V_{mnl}^{MM} = \sqrt{\frac{Y_{mn}^{i+1, TM}}{Y_{kl}^{i, TM}}} \int_{A^i} \bar{e}_{kl}^{i, TM} \cdot \bar{e}_{mn}^{i+1, TM} dA^i. \quad (31)$$

The orthonormalized modal eigenfunctions for section $\#(i+1)$ of Fig. 2 have the explicit form:

$$\bar{e}_{mn}^{i+1, TE} = A_{mn}^{i+1} \{ k_{ym}^{i+1} \cos(k_{xm}^{i+1} x) \sin(k_{yn}^{i+1} y) x - k_{xm}^{i+1} \sin(k_{xm}^{i+1} x) \cos(k_{yn}^{i+1} y) y \} \quad (32)$$

$$\bar{e}_{mn}^{i+1, TM} = A_{mn}^{i+1} \{ k_{xm}^{i+1} \cos(k_{xm}^{i+1} x) \sin(k_{yn}^{i+1} y) x + k_{yn}^{i+1} \sin(k_{xm}^{i+1} x) \cos(k_{yn}^{i+1} y) y \} \quad (33)$$

where

$$k_{xm} = \frac{m\pi}{x^{i+1}} \quad k_{yn} = \frac{n\pi}{y^{i+1}} \quad (34)$$

and A_{mn}^{i+1} is a normalization constant.

B. Matching to Half-Space

The matrix F of (8) has elements which are summations of three kinds of integrals as described below:

$$I_{1ijmn}^{pq} = \frac{W_{ij}^p W_{mn}^q}{2\pi} \int_{-x_N}^{x_N} \int_{-y_N}^{y_N} \left\{ \frac{ie^{-ik\rho}}{\rho} \left(k^2 + \frac{\partial^2}{\partial y^2} \right) \cdot [R_{im}^{cc}(x) R_{jn}^{ss}(y)] \right\} dx dy \quad (35)$$

$$I_{2ijmn}^{pq} = \frac{U_{ij}^p U_{mn}^q}{2\pi} \int_{-x_N}^{x_N} \int_{-y_N}^{y_N} \left\{ \frac{ie^{-ik\rho}}{\rho} \left(k^2 + \frac{\partial^2}{\partial y^2} \right) \cdot [R_{im}^{ss}(x) R_{jn}^{cc}(y)] \right\} dx dy \quad (36)$$

$$I_{3ijmn}^{pq} + \frac{-1}{2\pi} \int_{-x_N}^{x_N} \int_{-y_N}^{y_N} \left\{ \frac{ie^{-ik\rho}}{\rho} \frac{\partial^2}{\partial x \partial y} \cdot \left[U_{ij}^p W_{mn}^q R_{mi}^{cs}(-x) R_{jn}^{cs}(y) + W_{ij}^p U_{mn}^q R_{im}^{cs}(x) R_{nj}^{cs}(-y) \right] \right\} dx dy. \quad (37)$$

In the above integrals, W and U are normalization coefficients and R_{ij}^{cs} denotes the convolution $R_{ij}^{cs} = \cos(k_{vi}v) \otimes \sin(k_{vj}v)$ over the aperture cross-section (X^N, Y^N) . The convolutions are evaluated analytically and the singularity at $\rho = 0$ is removed by performing the integrations on the polar plane. Romberg's method is used to compute numerically the integrations [13].

- 1) Indexes p and q take their values in the set $\{1, 2\}$, 1 denotes a TE mode whereas 2 denotes a TM mode.
- 2) Indexes i, j and m, n take their values in the set $\{0, 1, 2, \dots, M\}$ where TE_{MM}, TM_{MM} is the highest order secondary mode included in the derivation of the Green's function.
- 3)

$$W_{ij}^p = \begin{cases} A_{ij}^{(N)} \left(\frac{j\pi}{y^N} \right) & \text{if } p = 1 \text{ (TE)} \\ A_{ij}^{(N)} \left(\frac{i\pi}{x^N} \right) & \text{if } p = 2 \text{ (TM)} \end{cases} \quad (38)$$

$$U_{ij}^p = \begin{cases} -A_{ij}^{(N)} \left(\frac{i\pi}{x^N} \right) & \text{if } p = 1 \text{ (TE)} \\ A_{ij}^{(N)} \left(\frac{j\pi}{y^N} \right) & \text{if } p = 2 \text{ (TM)}. \end{cases} \quad (39)$$

The explicit form of the matrix F defined by (8) can now be described as follows:

$$F = [F_{11} \quad F_{22}]$$

where the block matrices F_{11}, F_{22} are of the form:

$$F_{11} = \begin{bmatrix} f^{11,+} & f^{12} \\ f^{21} & f^{22,+} \end{bmatrix} \quad F_{22} = \begin{bmatrix} f^{11,-} & f^{12} \\ f^{21} & f^{22,-} \end{bmatrix} \quad (40)$$

and

$$\begin{cases} \sqrt{Y_{ij}^{N,q}} f_{ijmn}^{qq\pm} = S_{ijmn}^{qq} \pm \delta_{im} \delta_{jn} Y_{mn}^{N,q} & \text{if } (q = p) \\ \sqrt{Y_{ij}^{N,q}} f_{ijmn}^{pq} = S_{ijmn}^{pq} & \text{if } (q \neq p) \end{cases} \quad (41)$$

where

$$S_{ijmn}^{pq} = \frac{1}{\omega \mu_0} \sum_{s=1}^3 I_{sijmn}^{pq} \quad (42)$$

and δ_{im} is the Kronecker delta.

REFERENCES

- [1] G. M. Rebeiz, D. P. Kasilingam, P. A. Stimson, Y. Guo, and D. B. Rutledge, "Monolithic millimeter-wave two-dimensional horn imaging arrays," *IEEE Trans. Antennas Propagat.*, vol. 38, pp. 1473-1482, Sept. 1990.
- [2] W. Y. Ali-Ahmad and G. M. Rebeiz, "92 GHz dual-polarized integrated horn antennas," *IEEE Trans. Antennas Propagat.*, vol. 39, pp. 820-825, July, 1991.
- [3] W. Y. Ali-Ahmad, G. V. Eleftheriades, L. P. B. Katehi, and G. M. Rebeiz, "Millimeter-wave integrated-horn antennas: Part II—Experiment," *IEEE Trans. Antennas Propagat.*, pp. 1582-1586, this issue.
- [4] Y. Guo, K. Lee, P. A. Stimson, K. A. Potter, and D. B. Rutledge, "Aperture efficiency of integrated-circuit horn antennas," *Microwave Opt. Tech. Lett.*, vol. 4, no. 1, pp. 6-9, Jan. 1991.
- [5] P. B. Katehi and N. G. Alexopoulos, "Frequency-dependent characteristics of microstrip discontinuities in millimeter-wave integrated circuits," *IEEE Trans. Microwave Theory Tech.*, vol. MTT-33, pp. 1029-1035, Oct. 1985.
- [6] W. P. Harokopos and P. B. Katehi, "Characterization of microstrip discontinuities on multilayer dielectric substrates including radiation losses," *IEEE Trans. Microwave Theory Tech.*, vol. 37, pp. 2085-2065, Dec. 1989.
- [7] L. P. Dunleavy and P. B. Katehi, "A generalized method for analyzing shielded thin microstrip discontinuities," *IEEE Trans. Microwave Theory Tech.*, vol. 36, pp. 1758-1766, Dec. 1988.
- [8] R. J. Jackson and D. M. Pozar, "Full-wave analysis of microstrip open-end and gap discontinuities," *IEEE Trans. Microwave Theory Tech.*, vol. MTT-33, pp. 1036-1042, Oct. 1985.
- [9] J. A. Encinar and J. M. Rebollar, "Hybrid technique for analyzing corrugated and noncorrugated rectangular horns," *IEEE Trans. Antennas Propagat.*, vol. AP-34, pp. 961-968, Aug. 1986.
- [10] T. Wriedt, K. Wolff, F. Arndt, and U. Tucholke, "Rigorous hybrid field theoretic design of stepped rectangular waveguide mode converters including the horn transitions into half-space," *IEEE Trans. Antennas Propagat.*, vol. 37, pp. 780-790, June 1989.
- [11] H. Patzelt and F. Arndt, "Double-plane steps in rectangular waveguides and their applications for transformer, irises, and filters," *IEEE Trans. Microwave Theory Tech.*, vol. MTT-30, pp. 771-776, May 1982.
- [12] R. H. MacPhie and A. I. Zaghoul, "Radiation from rectangular waveguide with infinite flange-Exact solution by the correlation matrix method," *IEEE Trans. Antennas Propagat.*, vol. AP-28, pp. 497-503, July 1980.
- [13] H. A. Lessow, W. V. T. Rusch, and H. Schjaer-Jacobson, "On numerical evaluation of two-dimensional integrals," *IEEE Trans. Antennas Propagat.*, vol. AP-23, pp. 714-718, Sept. 1975.
- [14] J. C. Maxwell, *A Treatise on Electricity and Magnetism*, 3rd ed., vol. 1. New York: Dover, 1954, pp. 296-297.
- [15] R. E. Collin, *Antennas and Radiowave Propagation*. New York: McGraw-Hill, 1985, pp. 284-286.



George V. Eleftheriades (S'88) was born in Limassol, Cyprus, in May 1963. He received the diploma in electrical engineering with distinction from the National Technical University of Athens, Athens, Greece, in 1988 and the M.S. degree in electrical engineering from the University of Michigan, Ann Arbor, in 1989.

Currently he is working toward the Ph.D. degree at the Radiation Laboratory of the University of Michigan. His research interests include millimeter-wave antennas and circuits, Gaussian-beam techniques, phased arrays and analytical techniques in electromagnetics.

Mr. Eleftheriades received the Best Paper Award at the 1990 International Conference on Antennas, Nice, France, and the "Distinguished Achievement Award," from the Department of Electrical Engineering of the University of Michigan, in February 1991.

Walid Y. Ali-Ahmad (S'89), for a photograph and biography please see page 825 of the June 1991 issue of this TRANSACTIONS.

Linda P. B. Katehi (S'81-M'84-SM'89), for a photograph and biography please see page 1045 of the July 1990 issue of the TRANSACTIONS.

Gabriel M. Rebeiz (S'86-M'88), for a biography please see page 825 of the June 1991 issue of this TRANSACTIONS.